SUPPLEMENTAL DATA

Temporal phosphoproteomics reveals circuitry of phased propagation in insulin signaling

Michael Turewicz[1,2#], Christine Skagen[3#], Sonja Hartwig[1,2], Stephan Majda[1,2], Kristina Thedinga[4], Ralf Herwig[4], Christian Binsch[1,2], Delsi Altenhofen[1,2], D. Margriet Ouwens[1,2,5], Pia Marlene Förster[1,2], Thorsten Wachtmeister[6], Karl Köhrer[6], Torben Stermann[1,2], Alexandra Chadt[1,2], Stefan Lehr[1,2], Tobias Marschall[7,8], G. Hege Thoresen[3,9], Hadi Al-Hasani[1,2*]

[1]Institute for Clinical Biochemistry and Pathobiochemistry, German Diabetes Center (DDZ), Leibniz Center for Diabetes Research at the Heinrich Heine University Düsseldorf, Medical Faculty, Düsseldorf, Germany

[2]German Center for Diabetes Research (DZD e.V.), München-Neuherberg, Germany

[3]Section for Pharmacology and Pharmaceutical Biosciences, Department of Pharmacy, University of Oslo, Oslo, Norway

[4]Department of Computational Molecular Biology, Max-Planck-Institute for Molecular Genetics, Berlin, Germany

[5]Department of Endocrinology, Ghent University Hospital, Ghent, Belgium

[6]Genomics and Transcriptomics Laboratory, Biologisch-Medizinisches-Forschungszentrum (BMFZ), Heinrich Heine University Düsseldorf, Düsseldorf, Germany

[7]Institute for Medical Biometry and Bioinformatics, Medical Faculty, Heinrich Heine University Düsseldorf, Düsseldorf, Germany

[8]Center for Digital Medicine, Heinrich Heine University Düsseldorf, Düsseldorf, Germany

[9]Department of Pharmacology, Institute of Clinical Medicine, University of Oslo, Oslo, Norway

#equal contribution

*Correspondence should be addressed to: Hadi Al-Hasani, Institute for Clinical Biochemistry and Pathobiochemistry, German Diabetes Center (DDZ), Leibniz Center for Diabetes Research at Heinrich Heine University, Auf'm Hennekamp 65, 40225 Düsseldorf, Germany (hadi-al-hasani@ddz.de)

Supplemental Figures

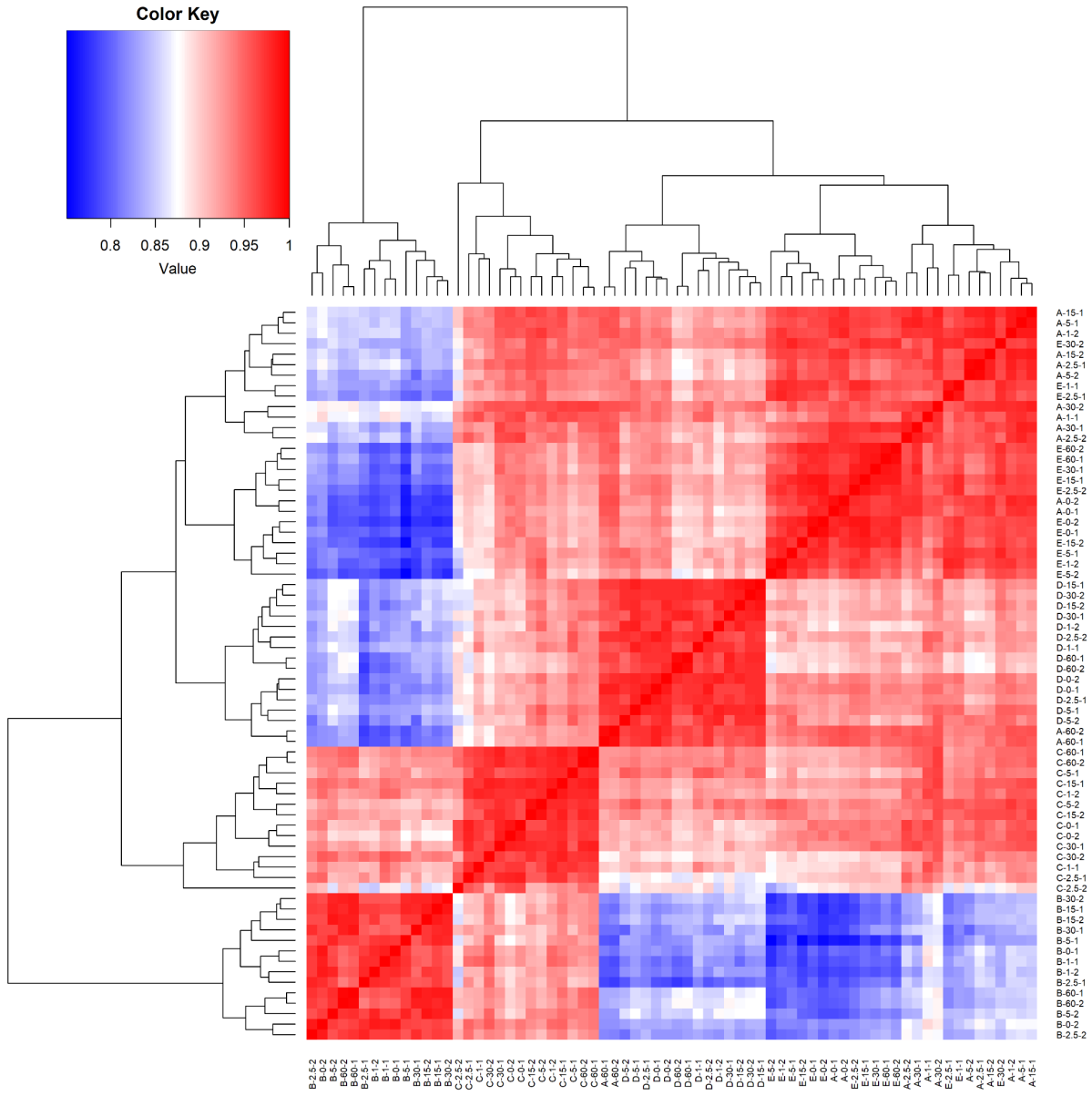

Supplemental Figure 1: Variation in the abundance of phosphopeptides between technical replicates for all five donors and seven time points. Abundance values of all 70 samples including all 5 donors (represented by A, B, C, D and E), all 7 time points and all pairs of technical replicates were used for hierarchical clustering (correlation-based distance metric).

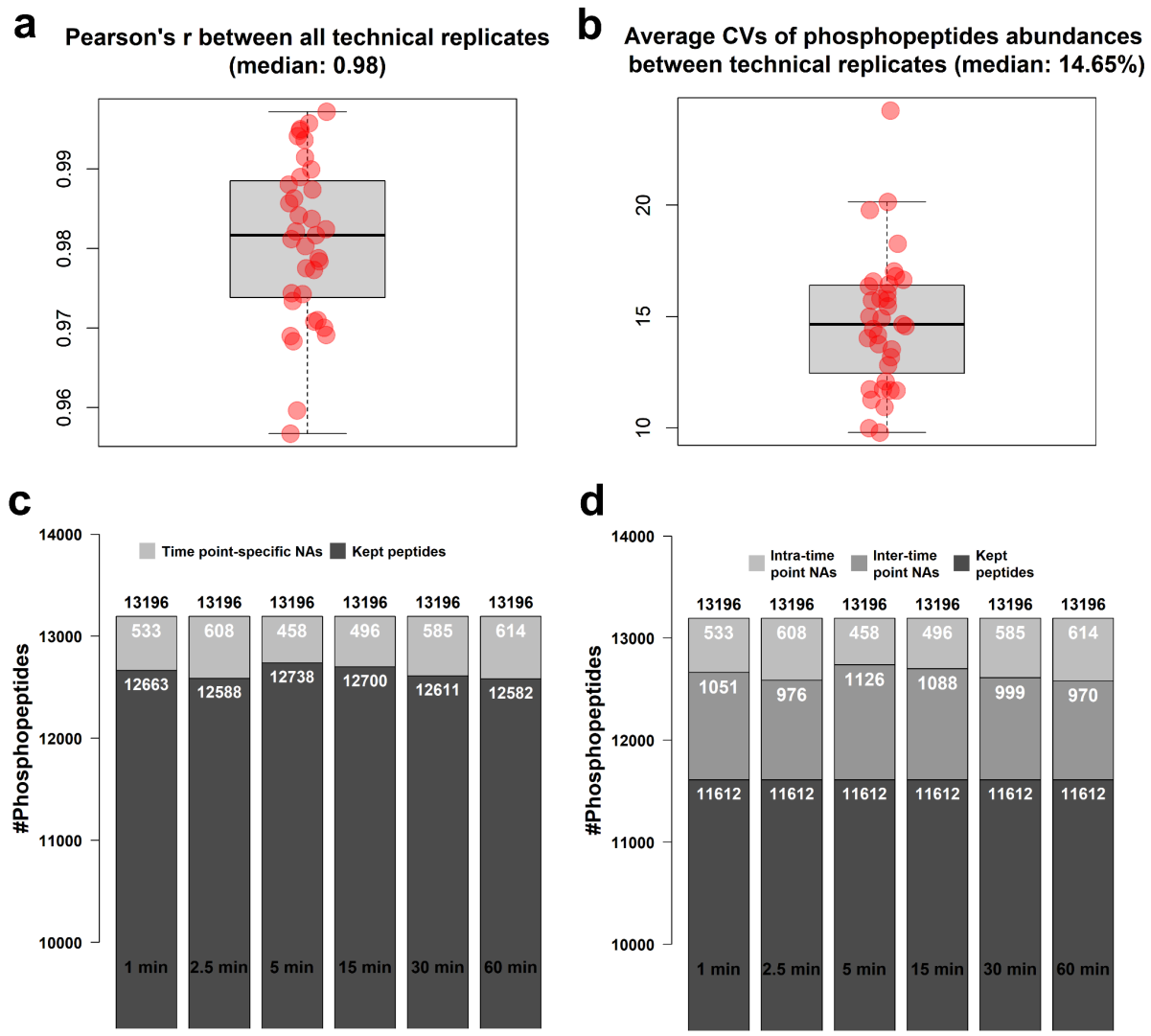

Supplemental Figure 2: Similarity, data reproducibility and comparability of the quantified phosphopeptides. a) Distribution of Pearson's r between the abundances of phosphopeptides of all 35 pairs of technical replicates for all five donors and all seven time points with the median value of r = 0.98. **b)** Distribution of coefficients of variation (CVs) computed in analogy to b) for all 35 pairs of technical replicates. **c)** Different numbers of various phosphopeptides with missing abundance values (NAs) within the time points after insulin stimulation ("time point-specific NAs" or "intra-time point NAs"). **d)** After removing all phosphopeptides that have at least one NA value in any other time point ("inter-time point NAs"), 11,612 phosphopeptides remain with quantitative data for at all time points. Median CV values for the 5 donors (A - E; 5x 11.612 phosphopeptides) were 0.2465 (A), 0.253 (B), 0.2486 (C), 0.2618 (D), 0.2149 (E). Median CV values for the 7 time points (1..60 min; 7x 11.612 phosphopeptides) were 0.2585 (1 min), 0.2678 (2.5 min), 0.2628 (5 min), 0.2697 (15 min), 0.2672 (30 min), 0.2879 (60 min).

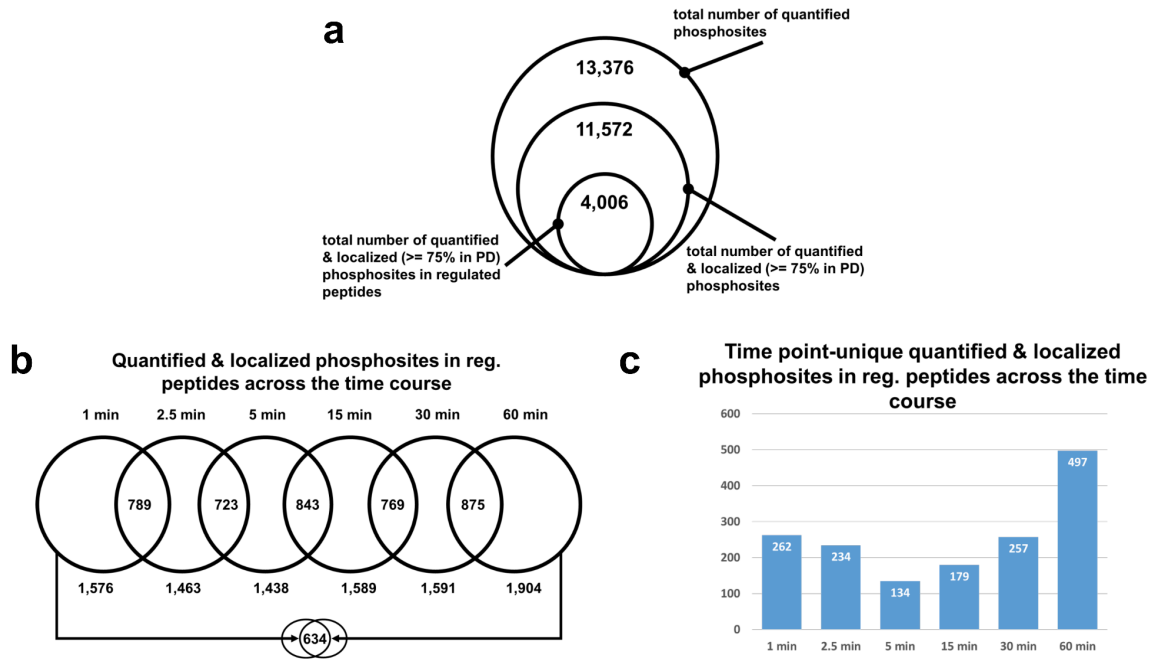

Supplemental Figure 3: Phosphosite numbers over time. a) Total number of phosphosites, number of class I phosphosites (i.e. ≥ 75% localization probability) and number of class I phosphosites in regulated peptides quantified within the entire data set. **b)** Time point-specific numbers of phosphosites in regulated peptides and their overlaps between adjacent time points. **c)** Numbers of time point-specific phosphosites in regulated phosphopeptides across the time course.

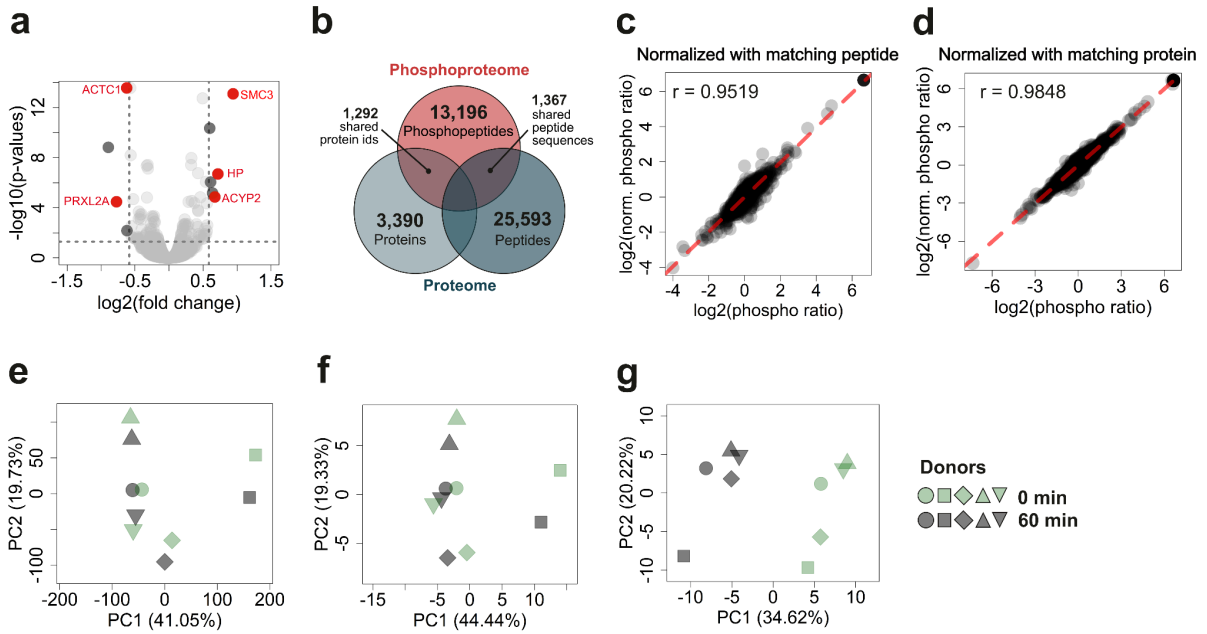

Supplemental Figure 4: Normalization using protein abundances and comparison of insulin-stimulated phosphoproteome and total proteome of human myotubes.

a) Changes in abundance of all 3,390 quantitated proteins in the total proteome from human myotubes after 60 min insulin stimulation (100 nM) relative to the basal state. **b)** Overlap between the quantified phosphoproteins in the phosphoproteome and proteins in the total proteome (1,292 shared UniProt IDs), as well as the quantified phosphopeptides in the phosphoproteome and peptides in the total proteome (1,367 shared peptide sequences). **c)** Correlation of phosphopeptide abundance value ratios (t_{60} vs. t_0) without and with normalization of phosphopeptide abundances based on abundances of peptides from the total proteome having identical amino acid sequences. This normalization was not possible for 11,829 phosphopeptides (89.6%) because no matching peptide was quantified in the total proteome. **d)** Correlation of 5,322 phosphopeptide abundance value ratios (t_{60} vs. t_0) without and with normalization of phosphopeptide abundances based on abundances of proteins from the total proteome having identical UniProt IDs. This normalization was not possible for 7,874 phosphopeptides (59.7%) because no matching protein was quantified in the total proteome. **e)** PCA of protein variance in the total proteome, **f)** PCA of a subset of non-phosphorylated peptides overlapping with sequences from enriched phosphopeptides in the phosphoproteome, **g)** PCA of regulated phosphopeptides found in the global proteome. Note that the abundance of the non-phosphorylated peptidoforms correlate mainly with donor identity whereas differentially phosphorylated peptides correlate with insulin treatment.

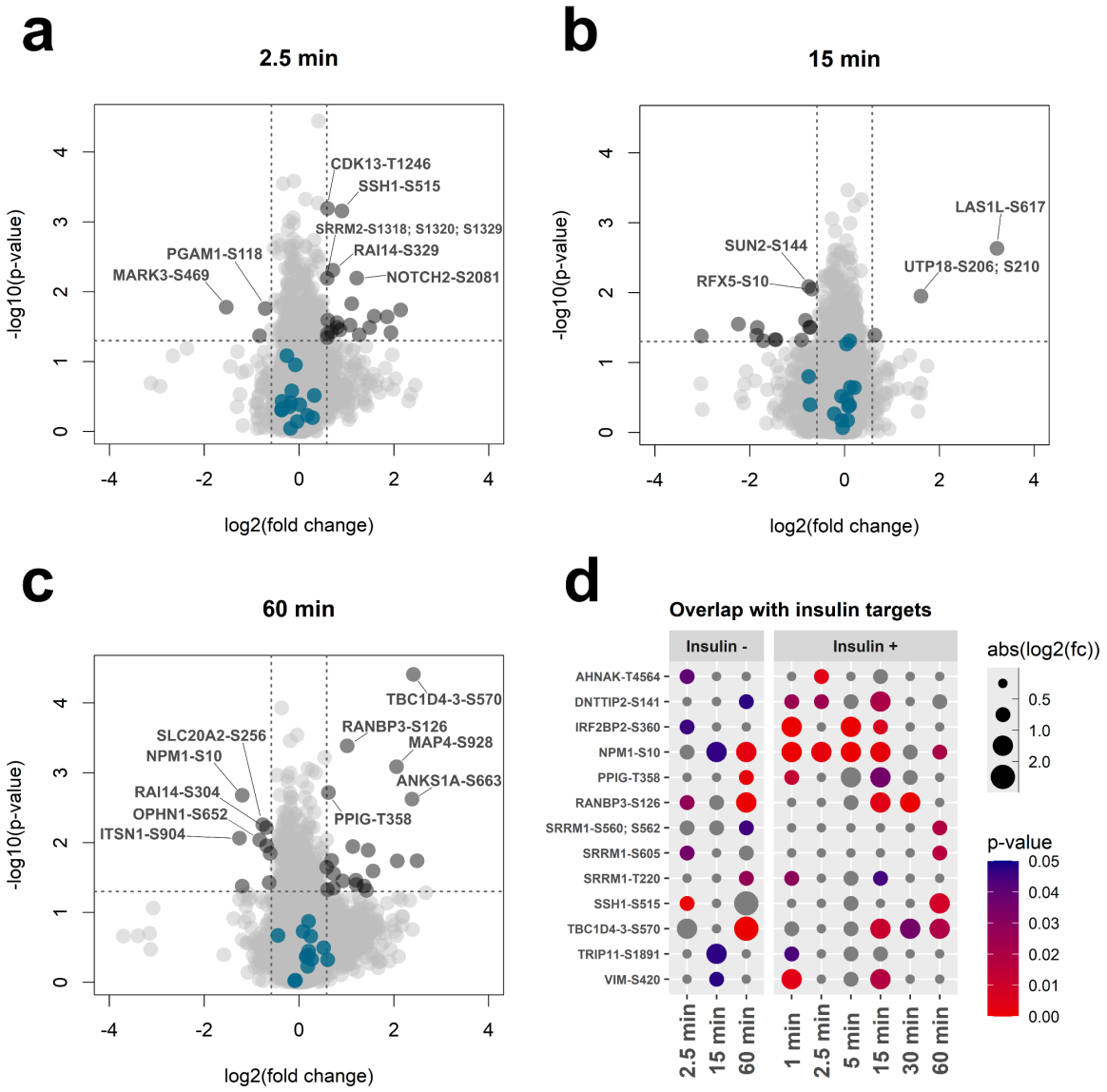

Supplemental Figure 5: Time-resolved phosphoproteomics analysis of human myotubes under starving conditions in the absence of insulin. Differentiated myotubes from three different donors were starved for 6 h. Subsequently, the cells were harvested at 0 min, 2.5 min, 15 min and 60 min and processed as described in Methods. The TiO2/Fe-IMAC- enriched tryptic phosphopeptides were quantified using mass spectrometry. **a-c)** Time point-specific volcano plots for phosphopeptides at baseline. A total of 61 phosphopeptides showed significant regulation ($p < 0.05$; $|FC| > 1.5$) at one or more time points during starvation. Phosphopeptides derived from canonical insulin targets (ACLY-S455, AKT1S1-T266, AKT2-T309, BAD-S75, CCDC88A-S1417, EIF4B-S422, MAPK1-T185, MAPK3-T202, MTOR-S2448, MYO5A-S1652, PDCD4-S457, PDCD4-S76, RPS6-S235; S236; S240, RPS6KA3-S369; S375) are marked in blue. **d)** Subset of phosphosites that are regulated under both, starving conditions in the absence of insulin as well as after insulin stimulation.

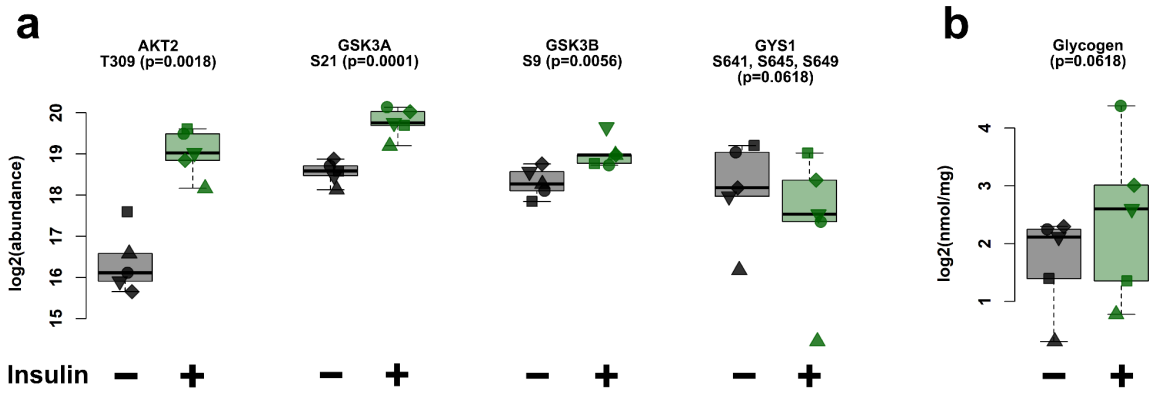

Supplemental Figure 6: Insulin regulated phosphorylation sites related to glycogen synthesis and glycogen levels in human myotubes. a) Abundance ratios of phosphopeptides in basal and insulin stimulated (100 nM, 60 min) cells from 5 donors. P-values relate to paired one-tailed t-test, adjusted according to Benjamini-Hochberg. **b)** Glycogen levels of the same donors before and after 180 min stimulation with insulin (paired one-sided t-test).

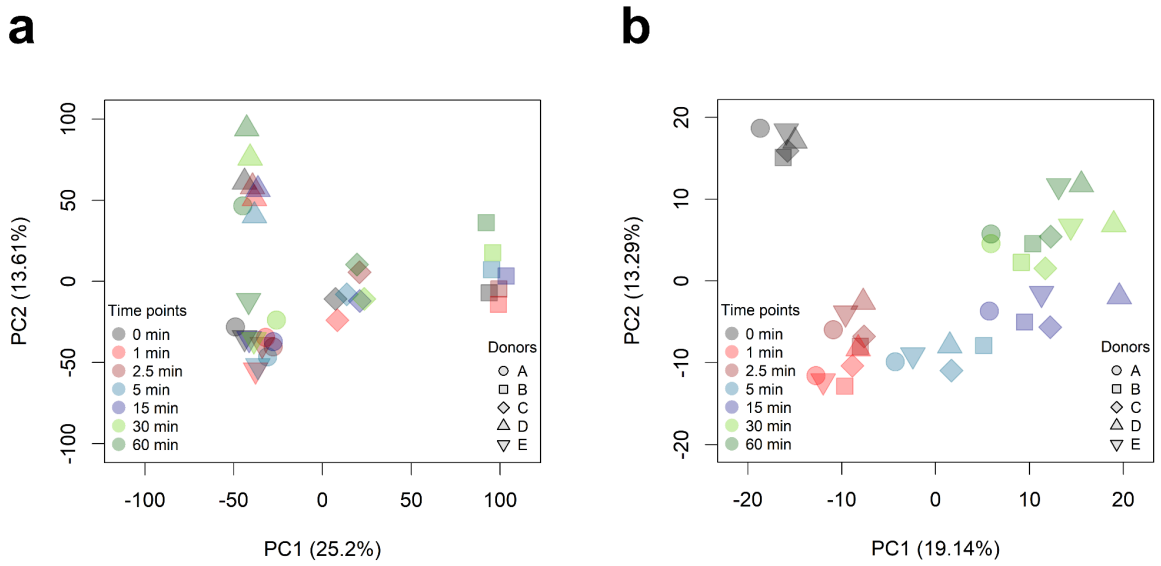

Supplemental Figure 7: Donor and time-dependent clustering of peptides and proteins in human myotubes. a) Principal component analysis (PCA) using abundance values of all 11,517 phosphopeptides that were quantified at all seven time points t_0 - t_{60} in each of the five donors represented by A - E. **b)** PCA using abundance values of 714 most differential phosphopeptides with p value < 0.01 and ratio against t_0 > 3 or < 1/3 that were quantified at all seven time points t_0 - t_{60} in all subjects represented by A - E.

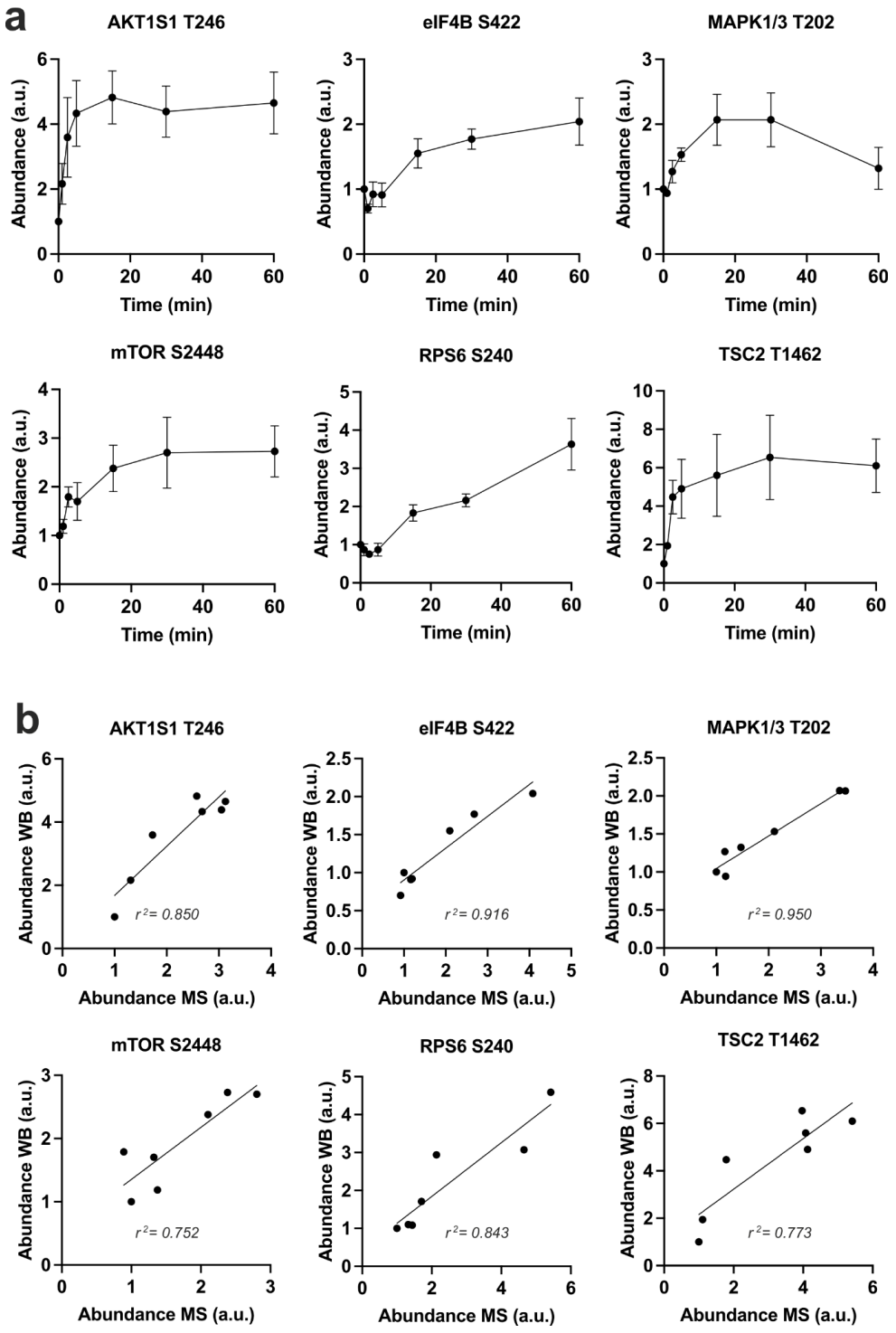

Supplemental Figure 8: Validation of phosphorylation kinetics of canonical AKT target sites. Human myotubes were stimulated with insulin (100 nM) for indicated times and analyzed for phosphorylation using Western Blot and mass spectrometry as described. **a)** Phosphorylation kinetics of AKT substrates quantified by Western blot analysis using phosphosite specific antibodies. **b)** Correlation of abundance values from Western blot analysis (WB) and mass spectrometry (MS). Data (mean, SEM) derived from analysis of 3-5 donors, coefficient of determination r^2 values from linear regression.

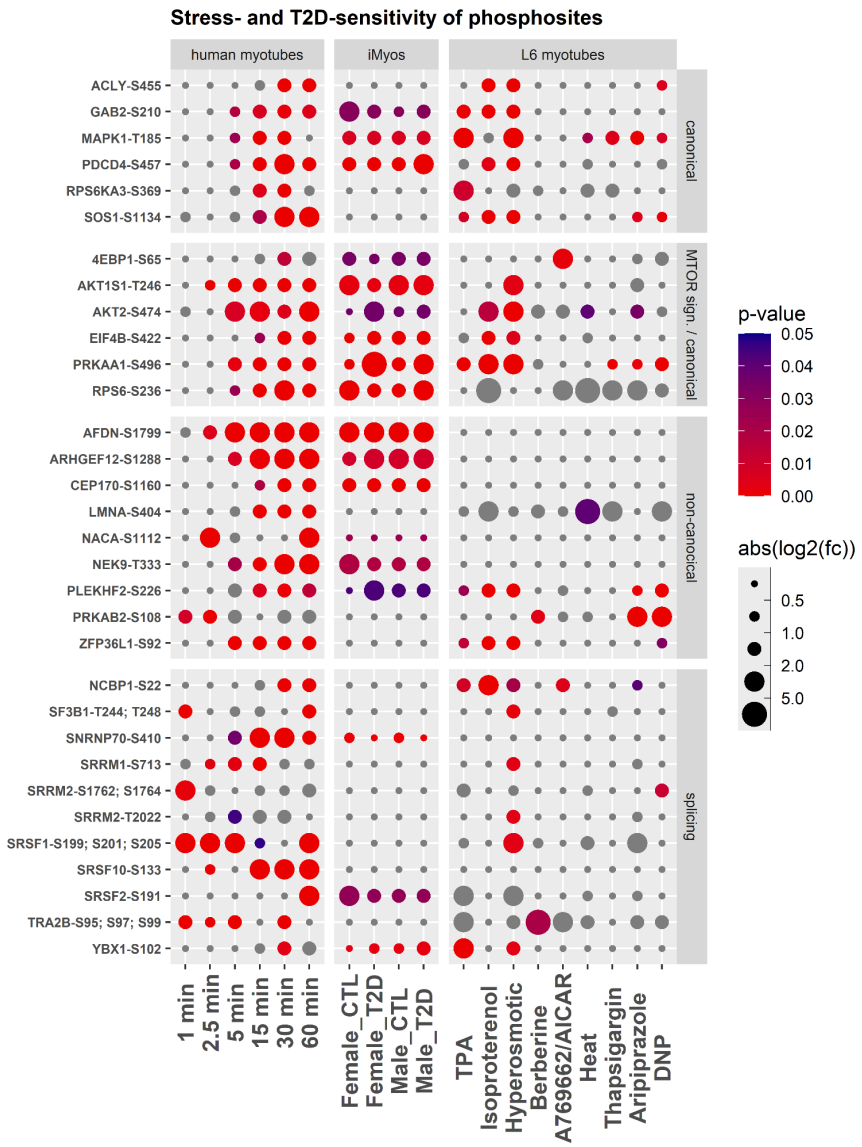

Supplemental Figure 9: Regulation of canonical and non-canonical phosphosites in stress-exposed, insulin-resistant muscle cells. Selected insulin-regulated phosphosites from human primary myotubes are compared with phosphorylation of corresponding sites in rat L6 myotubes treated with multiple stressors mimicking aspects of exercise [1], and insulin-stimulated (100 nM, 10 min) myoblasts derived from donors with T2D and healthy controls [2]. Fold changes refer to unstimulated control conditions. Only monophosphorylated peptides were considered for comparison. Ortholog mapping of phosphosites (rat, human) was conducted manually using UniProt and PhosphoSitePlus databases.

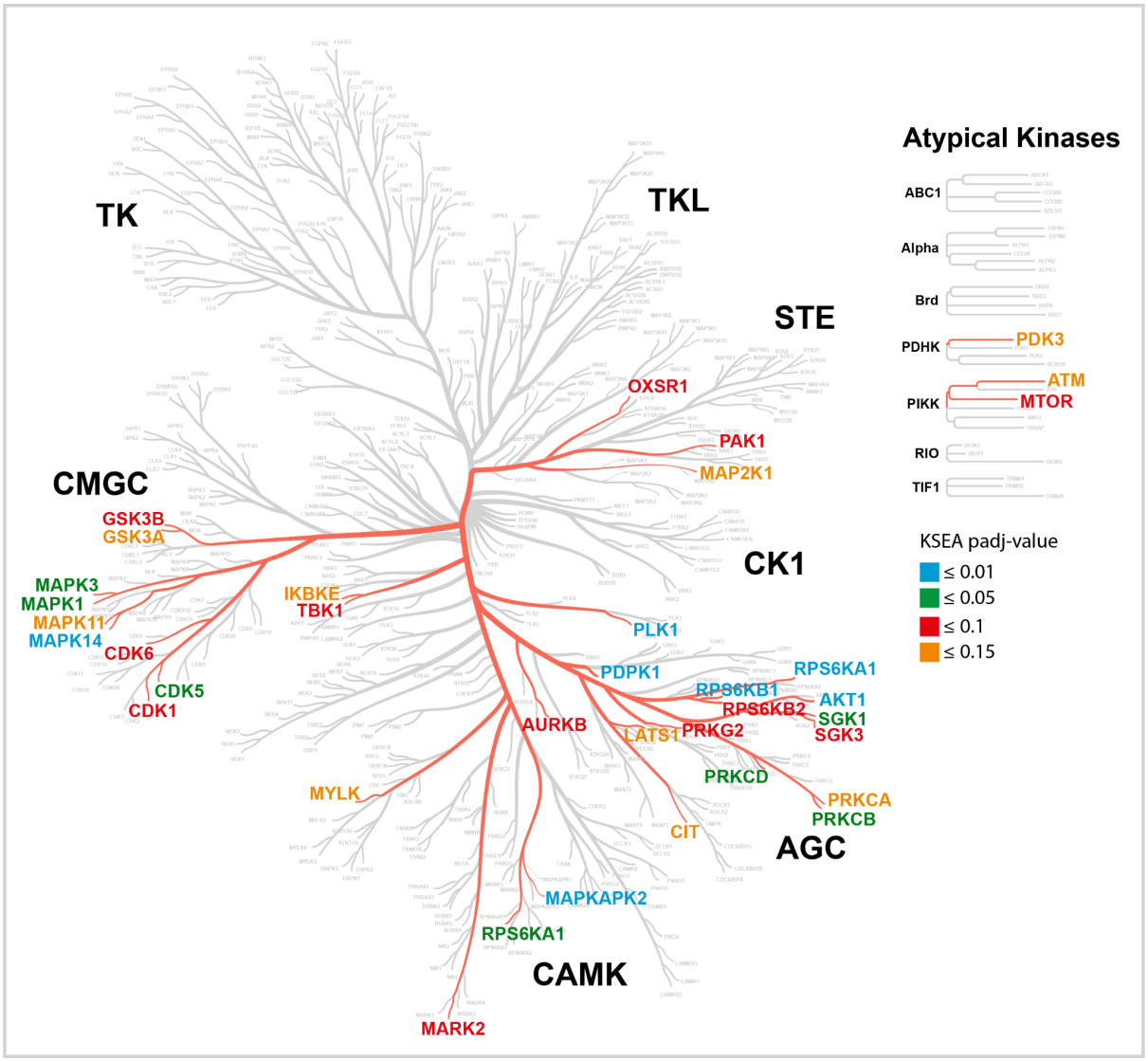

Supplemental Figure 10: Phylogenetic relations between insulin-stimulated kinases. Kinase set enrichment analysis (KSEA) of 4,030 insulin-regulated phosphopeptides from human primary myotubes was conducted as described in Methods. Overrepresented kinases and the respective p-values are indicated in the phylogenetic kinase family tree, along with annotations of the seven canonical kinase family subgroups [3].

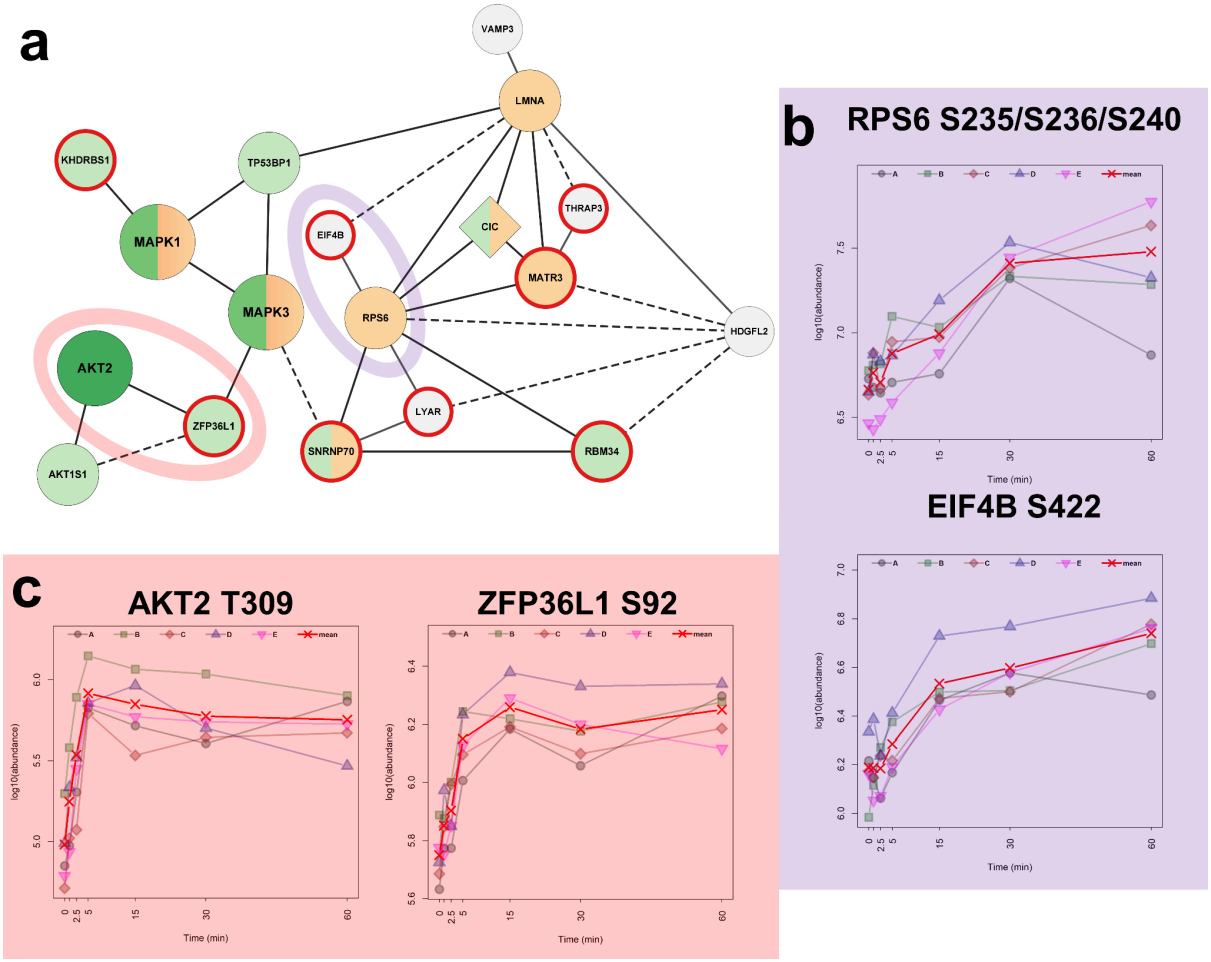

Supplemental Figure 11: Similarity of phosphorylation kinetics in PPI subnetwork. a) PPI subnetwork of phosphoproteins with low donor variability and similar phosphorylation kinetics. Nodes represent proteins with lowest inter-donor variability (mean of Pearson's *r* between all donors > 0.78), edges indicate similar phosphorylation kinetics of phosphopeptides with low variability (mean of Pearson's *r* between all donors > 0.73). Shown are protein kinases (green) and phosphatases (orange), and their respective first degree protein-protein interaction neighbors (light colors). RNA-binding proteins are marked in red. Dotted lines connect proteins with highly similar phosphorylation kinetics (Pearson's *r* > 0.9). **b)** The phosphorylation kinetics of a pair of phosphopeptides of RPS6 and EIF4B are shown as an example for the similarity of the phosphorylation kinetics of at least one pair of phosphopeptides of proteins directly connected by an edge in the PPI subnetwork. **c)** As another example, the phosphorylation kinetics of a pair of phosphopeptides of AKT2 and ZFP36L are visualized.

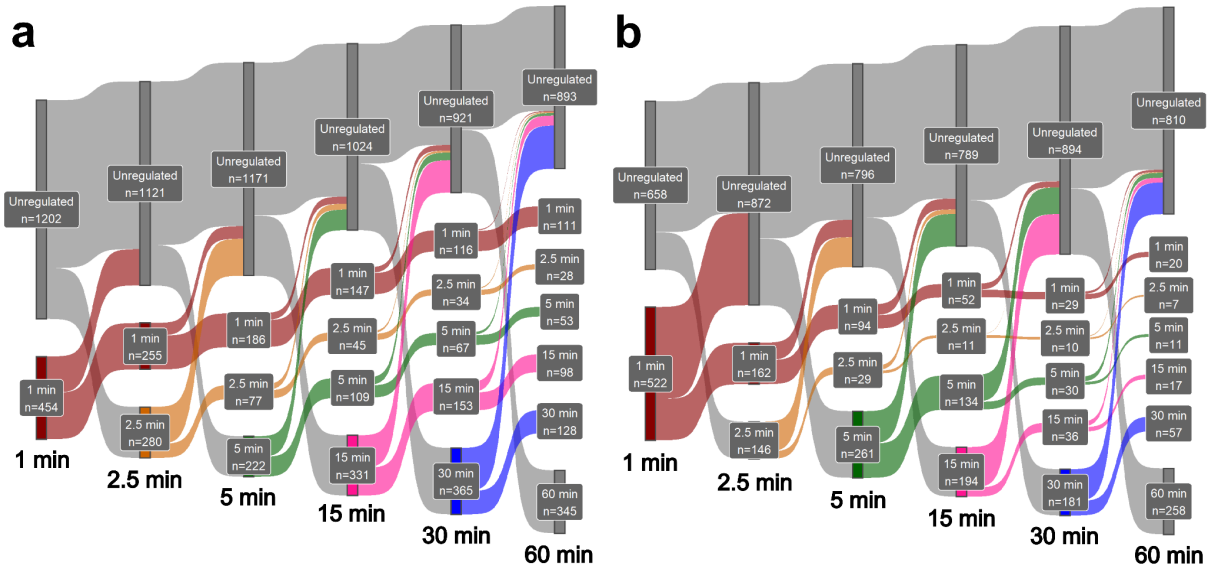

Supplemental Figure 12: Temporal dynamics of phosphopeptide regulation. Flow diagrams show phosphosite occupancy for **a)** 1,656 unique phosophopeptides upregulated in response to insulin and **b)** 1,180 unique phosophopeptides downregulated in response to insulin. Each phosphopeptide is represented by a single line where the colors denote the initial time point of continuous differential phosphorylation in response to insulin (| FC |> 1.3 *vs.* baseline; p <0.05). Lines aggregate continuous and discontinuous differential phosphorylation of individual peptides over time. Numbers in boxes indicate the numbers of unregulated (top level) and differentially phosphorylated peptides for each time point.

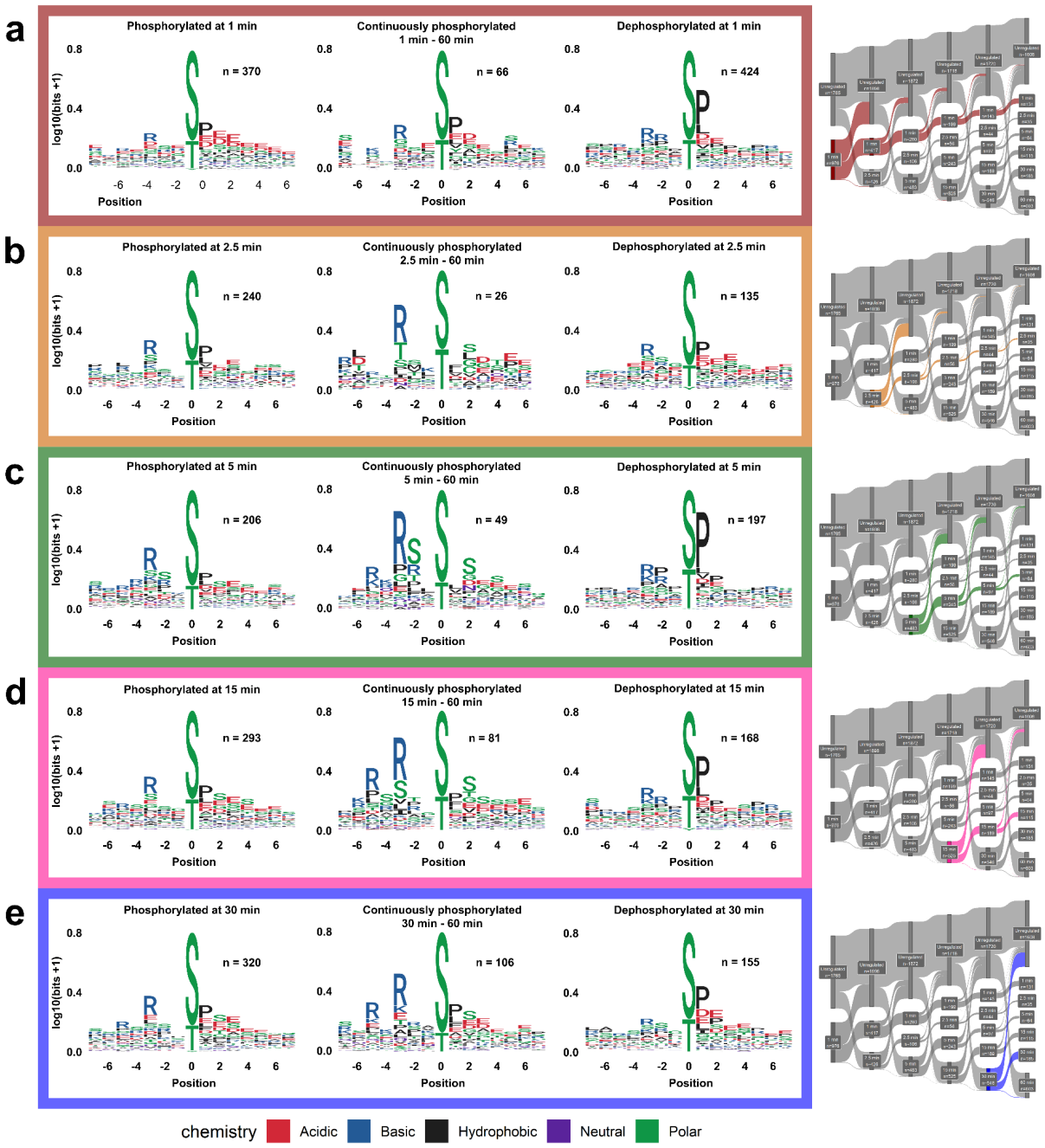

Supplemental Figure 13: Time-dependent consensus sequences of phosphosites regulated by insulin. Phosphosite motif analysis was conducted with phosphopeptides quantitated 1, 2.5 min, 5 min, 15 min, 30 and 60 min after insulin stimulation. Denoted are consensus sequences for phosphorylation and dephosphorylation at indicated time points, as well as motifs of continuously phosphorylated sites for indicated time intervals. The frequency of residues surrounding the phosphorylated residue is indicated by the size of the letters, as described in Methods; color code of subfigures a) - e) matches Supplemental Figure 12.

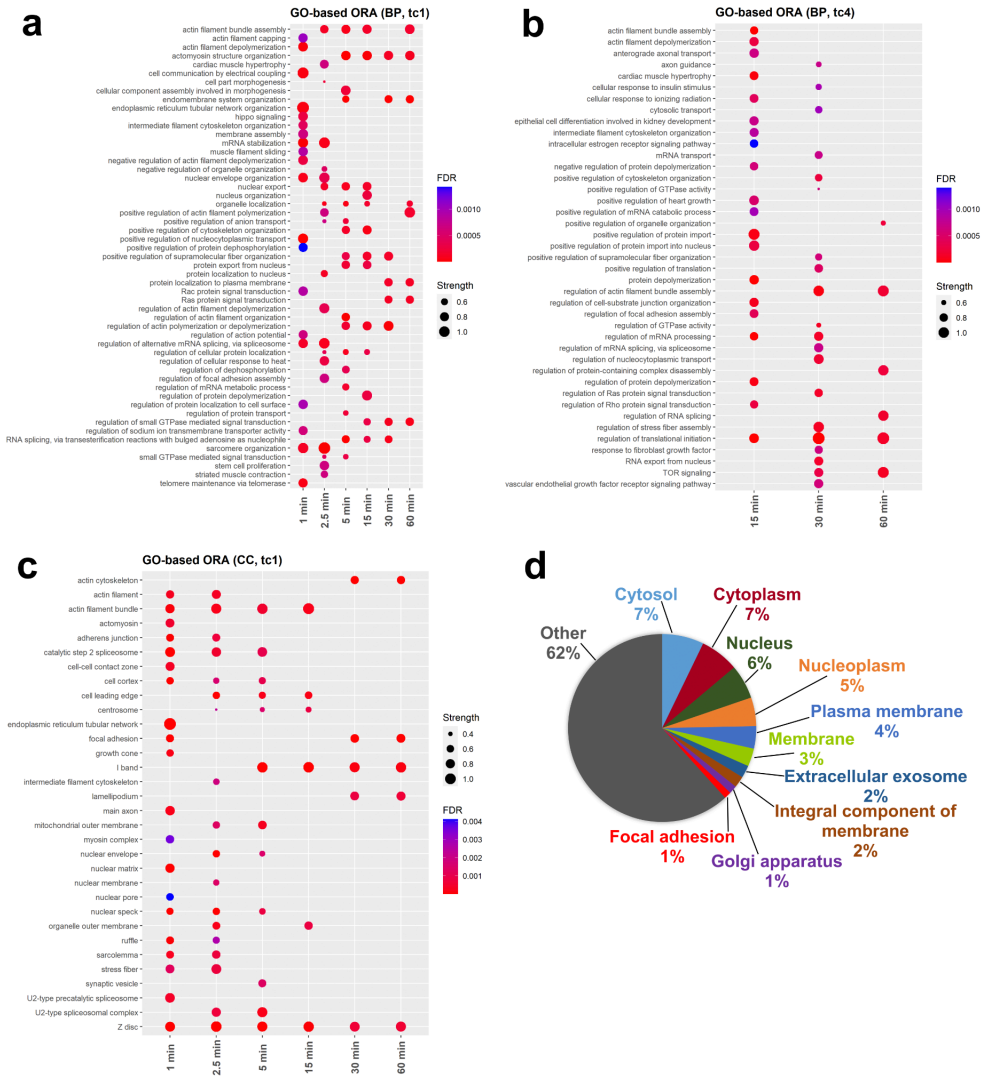

Supplemental Figure 14: Gene Ontology (GO)-based analysis. For all time-specific subsets of up- or downregulated phosphopeptides shown in the color-coded strands of the flow diagrams shown in Supplemental Figure 12 and visualizing temporal dynamics of phosphopeptide up- or downregulation, GO-based overrepresentation analysis (ORAs) was performed. Selected examples of respective ORA results are shown here. **a)** Significantly overrepresented pathways from "Biological Process (BP)"-based ORA for 454 phosphopeptides upregulated at t_1 (first node of the red strand in the upregulation-specific flow diagram). **b)** Significantly overrepresented pathways from BP-based ORA for 331 phosphopeptides newly upregulated at t_{15} (first node of the pink strand in the upregulation-specific flow diagram). **c)** Significantly overrepresented cellular components from "Cellular Component (CC)"-based ORA for 454 phosphopeptides upregulated at t_1 (first node of the red strand from the upregulation-specific flow diagram). **d)** Proportions of GO terms from the Cellular Component domain used to annotate the proteins of all phosphopeptides regulated at at least one time point in the entire dataset.

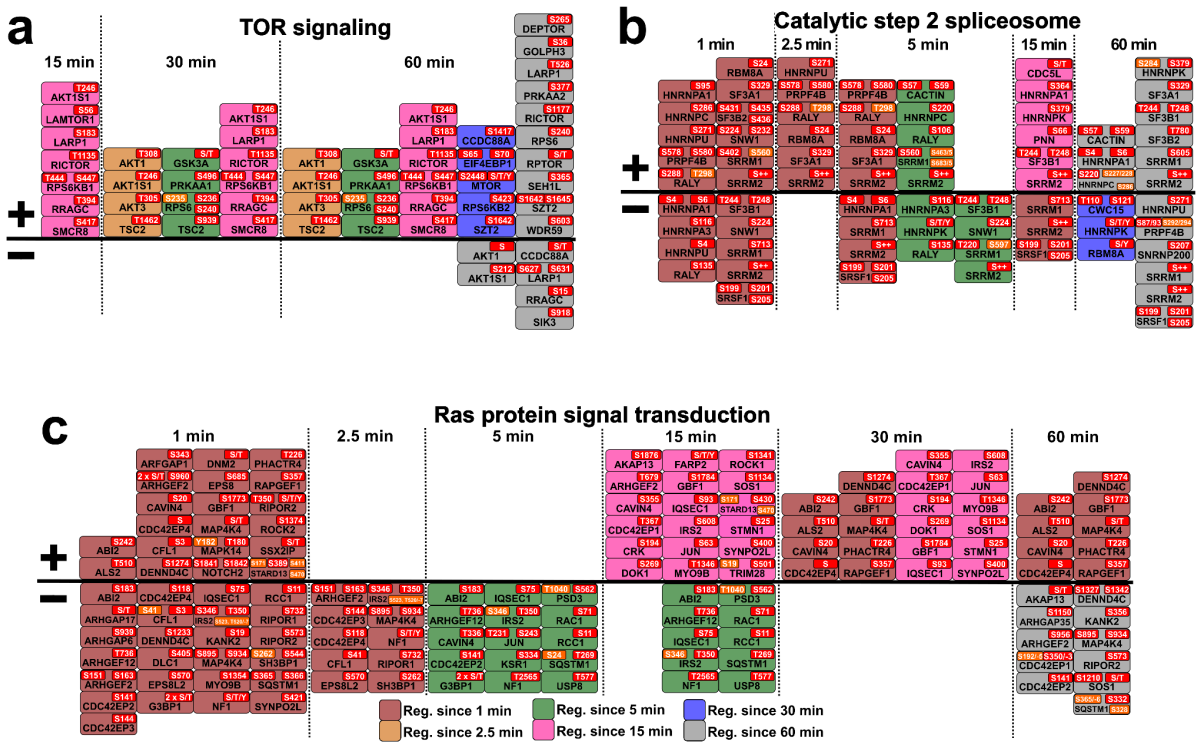

Supplemental Figure 15: Relative phosphosite occupancy of Ser/Thr residues in proteins significantly overrepresented in selected Gene Ontology (GO) pathways. For all time-specific subsets of up- or downregulated phosphopeptides shown in the color-coded strands of the flow diagrams shown in Supplemental Figure 12 and visualizing temporal dynamics of phosphopeptide up- or downregulation, GO-based overrepresentation analysis (ORAs) was performed. Three selected GO pathways that are overrepresented at multiple time points across the time course are visualized in subfigures a) - c). Residues are not shown at a particular time point when they are not significantly overrepresented there. Color code matches Supplemental Figure 12. **a)** TOR signaling. **b)** Catalytic step 2 spliceosome. **c)** Ras protein signal transduction.

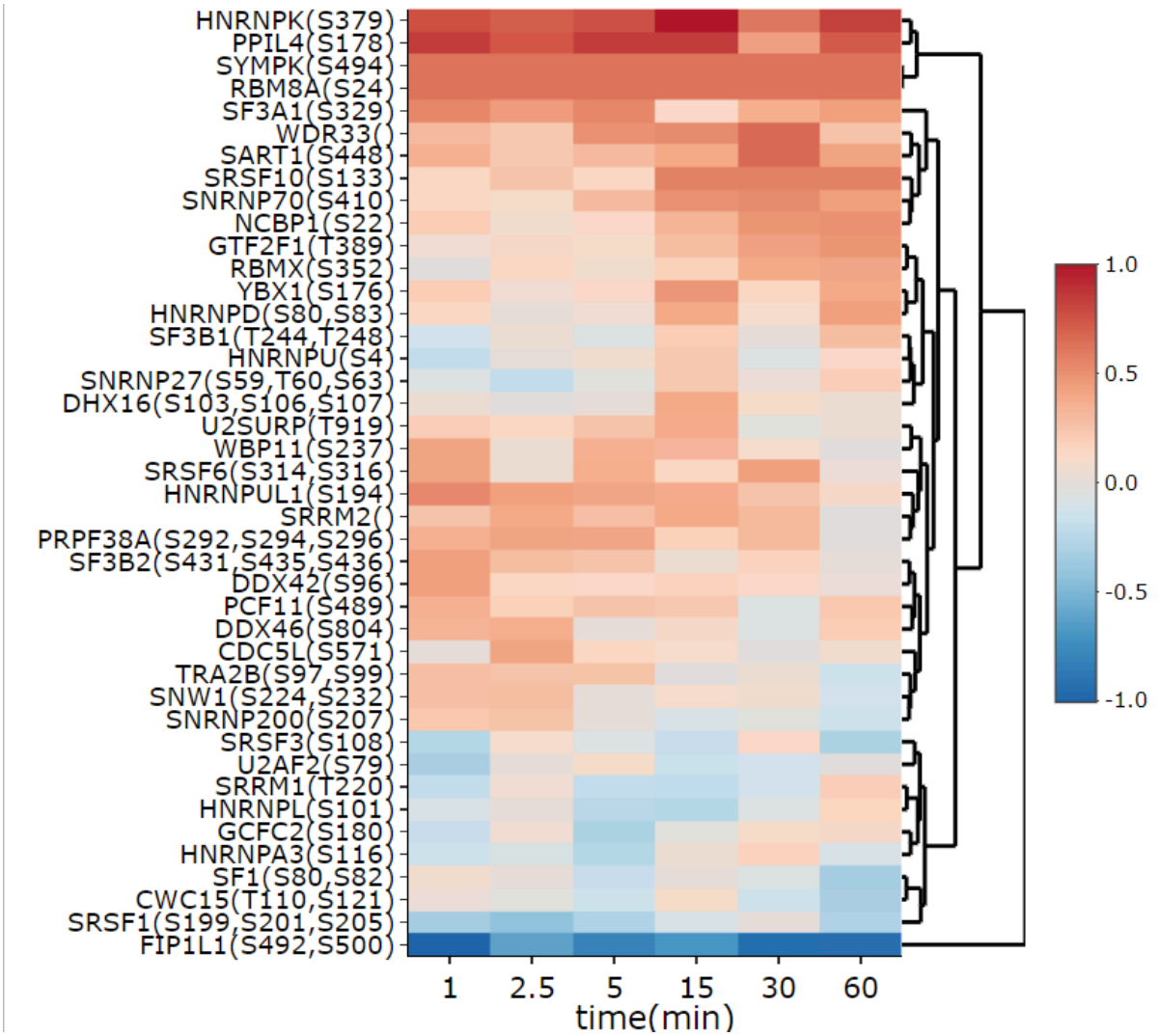

Supplemental Figure 16: Differential phosphorylation of spliceosomal proteins over time. Indicated are relative phosphosite occupancies of Ser/Thr residues in 42 spliceosomal and spliceosome-associated proteins. Proteins were selected if they were at any time point significantly different from the basal time point t_0.

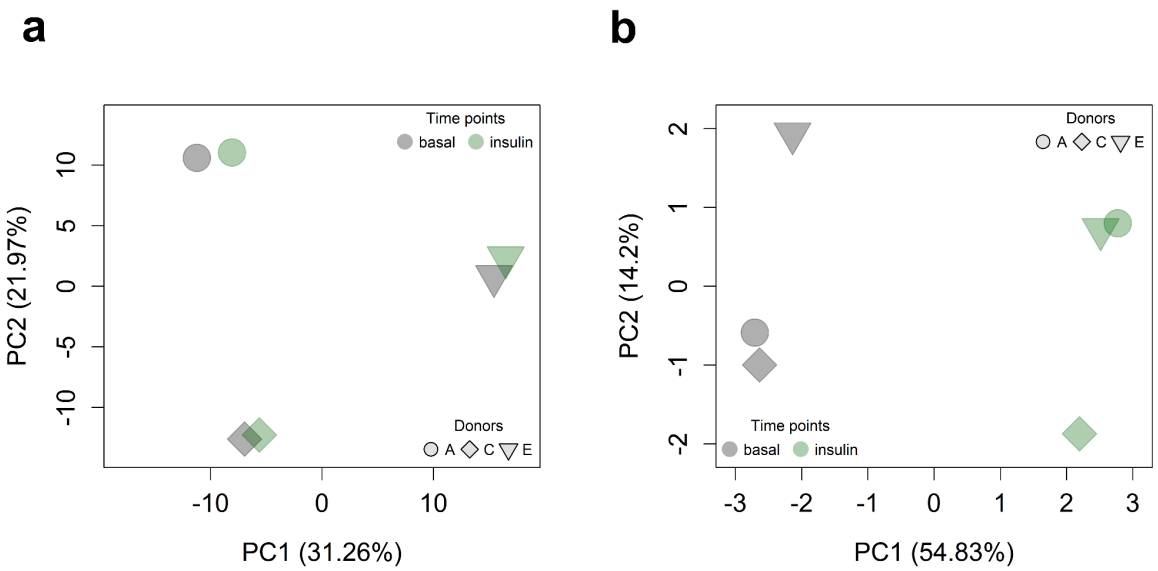

Supplemental Figure 17: Donor and insulin-dependent clustering of alternative RNA splicing events in human myotubes. a) Principal component analysis (PCA) using percent spliced in (PSI) values of all 1,192,998 alternative splicing (AS) events determined in myotubes from three donors (represented by symbols) before and after 60 min stimulation with insulin. **b)** PCA using differential splicing events between basal and insulin stimulated myotubes (adjusted p-value <= 0.05 and delta PSI t_{60} vs. t_0 >= 0.1). Alternative splicing was analyzed using multivariate analysis of transcript splicing (MATS) as described in Methods.

Supplemental Tables

Supplemental Table 1: Characteristics of human satellite cell donors.

Donor	VO_2max (ml/kg/min)	Fasting serum glucose (mmol/L)	Fasting serum Insulin (pmol/L)	Fasting serum C-peptide (pmol/L)	HOMA-IR
1	61.3	5.1	85	346	3.2
2	66.2	4.2	21	281	0.7
3	44.9	5.5	45	320	1.8
4	40.3	5.1	62	379	2.3
5	42.9	4.2	44	327	1.4
Mean (SD)	51.1 (10.5)	4.8 (0.5)	51.4 (21.3)	331 (32)	1.9 (0.8)

All procedures performed in studies involving human participants were in accordance with the ethical standards of Regional Committee for Medical and Health Research Ethics (REK) South East, Oslo, Norway (reference number 2011/2207). The donors were healthy men with mean values (± SD) for age: 24 (± 2.3) years; body weight: 83.10 (±4.6) kg; body height: 184 (± 3.9) cm; body mass index (BMI): 24.6 (± 1.7) kg/m^2; body fat mass: 13.1 (± 5.5) kg; and lean body mass: 69.1 (± 3.3) kg. The participants were fasted overnight before taking blood samples. There were no specific restrictions regarding exercise behavior during the study. Measurement of VO_2max was performed on a Monark Ergomedic 839E cycle (GIH, Stockholm, Sweden) as described [4]. Body composition was determined using Bio-electrical Impedance Analysis (InBody720; Biospace Co., Ltd. Seoul, Korea). HOMA-IR, Homeostatic Model Assessment for Insulin Resistance was calculated using the formula: (fS-glucose [in mmol/L]*fS-insulin [in pmol/L])/135; *n.d.*, not determined.

Supplemental Table 2: Insulin-regulated protein abundance in primary human myotubes.

Gene Symbol	Accession	Description	Fold change	Adj. p-value
IGK	P0DOX7	Immunoglobulin kappa light chain	1.515	4.48937E-11
FGG	P02679	Fibrinogen gamma chain	1.527	8.80612E-07
HP	P00738	Haptoglobin	1.646	1.99942E-07
IGHA1	P01876	Immunoglobulin heavy constant alpha 1	1.558	6.66317E-06
ACYP2	P14621	Acylphosphatase-2	1.596	1.35933E-05
SMC3	Q9UQE7	Structural maintenance of chromosomes protein 3	1.921	8.06527E-14
ACTC1	P68032	Actin, alpha cardiac muscle 1	0.649	2.72978E-14
PRXL2A	Q9BRX8	Peroxiredoxin-like 2A	0.585	3.28069E-05
DEFB103A; DEFB103B	P81534	Beta-defensin 103	0.538	1.50827E-09
TNFAIP8	O95379	Tumor necrosis factor alpha-induced protein 8	0.651	0.006633607

Basal and insulin stimulated (100 nM, 60 min) cells from 5 donors were harvested and analyzed for the global proteome as described (t-test p-values were adjusted using the method of Benjamini-Hochberg).

Supplemental Table 3: Proteins related to differentially phosphorylated peptides after 1 min of insulin-stimulation.

Upregulated genes (Uniprot ID)				Down regulated genes (Uniprot ID)
ABI2 (Q9NYB9)	EPS15L1 (Q9UBC2)	NAV1 (Q8NEY1)	RBM8A (Q9Y5S9)	ACTA1; ACTC1 (P68133; P68032)
AHNAK (Q09666)	ESYT1 (Q9BSJ8)	NAV2 (Q8IVL1)	REEP2 (Q9BRK0)	AKAP12 (Q02952)
ALS2 (Q96Q42)	FAM83H (Q6ZRV2)	NOP2 (P46087)	RILPL1 (Q5EBL4)	CASK (O14936)
ANKIB1 (Q9P2G1)	FERMT2 (Q96AC1)	NR3C1 (P04150)	RTN4 (Q9NQC3)	FIP1L1 (Q6UN15)
ANKLE2 (Q86XL3)	FKBP15 (Q5T1M5)	NUP88 (Q99567)	SAP30BP (Q9UHR5)	GOLIM4 (O00461)
ARHGAP22v (Q7Z5H3)	FRMD6 (Q96NE9)	PACS1 (Q6VY07)	SEPTIN4 (O43236)	HSPB6 (O14558)
ARHGAP39 (Q9C0H5)	GAB2 (Q9UQC2)	PDE4DIP (Q5VU43)	SH3RF1 (Q7Z6J0)	IRS2 (Q9Y4H2)
ASAP3 (Q8TDY4)	GBF1 (Q92538)	PDLIM1 (O00151)	SHANK2 (Q9UPX8)	LMOD3 (Q0VAK6)
ATF2 (P15336)	HERC1 (Q15751)	PDPK1 (O15530)	SMTN (P53814)	MAP2 (P11137)
ATOX1 (O00244)	IRGQ (Q8WZA9)	PEAR1 (Q5VY43)	SPAG9 (O60271; O60271)	NAV1 (Q8NEY1)
AZI2 (Q9H6S1)	KHDRBS1 (Q07666)	PHACTR4 (Q8IZ21)	SPTBN1 (Q01082; Q01082)	PEAR1 (Q5VY43)
BIN1 (O00499; O00499)	LARP1 (Q6PKG0)	PHF2 (O75151)	STK38L (Q9Y2H1)	PKM (P14618; P14618)
CAVIN4 (Q5BKX8)	LIMA1 (Q9UHB6; Q9UHB6)	PHLDB1 (Q86UU1)	STX16 (O14662)	PML (P29590; P29590; P29590)
CDC42EP4 (Q9H3Q1)	LMO7 (Q8WWI1)	PHRF1 (Q9P1Y6)	STX4 (Q12846)	SH3BP1 (Q9Y3L3)
CDV3 (Q9UKY7)	LNPK (Q9C0E8)	PKP4 (Q99569)	SYMPK (Q92797)	SLC19A3 (Q9BZV2)
CEBPB (P17676)	LPIN1 (Q14693)	PLEKHA5 (Q9HAU0)	SYNRG (Q9UMZ2)	TMSB4X (P62328)
CEP170B (Q9Y4F5)	LUC7L2 (Q9Y383)	PPIP5K1 (Q6PFW1)	TNRC6B (Q9UPQ9)	TNKS1BP1 (Q9C0C2)
CFL2 (Q9Y281)	MAP3K3 (Q99759)	PPP1R7 (Q15435)	TNS1 (Q9HBL0)	YTHDC1 (Q96MU7)
CHD4 (Q14839)	MAP4K4 (O95819)	PRPF4B (Q13523)	TP53BP1 (Q12888)	
CRACD (Q6ZU35)	MAPKAPK2 (P49137)	PRUNE2 (Q8WUY3)	TSC22D2 (O75157)	
CRIP2 (P52943)	MARCKS (P29966)	PSMG1 (O95456)	TXNIP (Q9H3M7)	
DDX20 (Q9UHI6)	MAST3 (O60307)	PTPDC1 (A2A3K4)	USP24 (Q9UPU5)	
DENND4C (Q5VZ89)	MATR3 (P43243)	RALGAPA2 (Q2PPJ7)	WDR44 (Q5JSH3)	
DYNC1I2 (Q13409)	MIA2 (Q96PC5)	RAPGEF1 (Q13905)	ZC3H18 (Q86VM9)	
EFR3A (Q14156)	MTOR (P42345)	RBFOX2 (O43251)	ZNF330 (Q9Y3S2)	
EPB41L1 (Q9H4G0)	MYO5A (Q9Y4I1)	RBM14 (Q96PK6)	ZNRF1 (Q8ND25)	

Supplemental Table 6: Proteins related to differentially phosphorylated peptides after 1 min of insulin-stimulation.

Supplemental Table 4: GLUT4-trafficking related proteins differentially phosphorylated after 1 min of insulin-stimulation.

Uniprot Accession	Gene name	Description	Annotated Peptide Sequence	Phosphorylated residue	Reference
O00499-10; O00499-2	BIN1	Isoform BIN1-13 of Myc box-dependent-interacting protein 1; Isoform IIB	[R].VNHEPEPAGGATPGATLPK.[S]	T307 ; T311 / O00499-10 T292; T296 / O00499-2	[5]
Q5VZ89-7	DENND4C	Isoform 2 of DENN domain-containing protein 4C	[K].LFSPVIAR.[N]	S1274	[6]
Q9BSJ8	ESYT1	Extended synaptotagmin-1	[R].LTHVDSPLEAPAGPLGQVK.[L]	T959, S963*	[7]
Q9Y4I1	MYO5A	Unconventional myosin-Va	[R].TSSIADEGTYTLDSILR.[Q]	S1652	[8]
Q86UU1	PHLDB1	Pleckstrin homology-like domain family B member 1	[R].RALSPLPTR.[T]	S470	[9]
Q2PPJ7	RALGAPA2	Ral GTPase-activating protein subunit alpha-2	[R].SATTSGAPGVEK.[A]	T715	[10]
Q13905-4	RAPGEF1/C3G	Isoform 4 of Rap guanine nucleotide exchange factor 1	[R].LSGGSHSYGGESPR.[L]	S357	[11]
Q12846	STX4	Syntaxin-4	[R].QGDDSSDEEDKER.[V]	S14; S15	[12]
O14662	STX16	Syntaxin-16	[R].SIAAELDELADDR.[M]	S41	[13]
Q9H3M7	TXNIP	Thioredoxin-interacting protein	[R].LESPTTPLLDDMDGSQDSPIFMYAPEFK.[F]	T349, S361*	[14]

* denotes manually localized phosphosites which were not unequivocally assigned by ProteomeDiscoverer.

Supplemental Table 5: Insulin-responsive gene expression in primary human myotubes.

HGNC Symbol	p-value	p-adj	fold change (FC)
ABCA7	7.05E-06	0.00933477	0.7346
DUSP2	1.08E-05	0.01229694	5.6523
EGR1	1.30E-06	0.00294801	6.2098
EGR3	3.31E-06	0.00519514	13.0452
FOS	2.66E-05	0.02483553	12.7230
FOXC2	3.60E-06	0.00519514	1.9890
GADD45B	1.41E-07	0.00055924	2.2990
GGNBP2	5.88E-05	0.04670993	1.1831
IER2	1.75E-05	0.0184885	4.0681
JMJD6	4.18E-05	0.0369095	1.8259
KCP	2.66E-06	0.00482503	1.7896
LIF	5.36E-07	0.00144704	3.3487
MIDN	5.46E-07	0.00144704	1.9389
MTA2	7.88E-08	0.00055924	1.3010
NR4A1	1.15E-07	0.00055924	26.9963
PHF23	2.54E-05	0.02483553	1.2552
PPRC1	6.59E-05	0.04984892	1.4874
SNAI1	2.73E-06	0.00482503	2.2656
ZC3H12A	8.21E-06	0.01003443	3.4877
ZNF304	5.30E-05	0.04434886	1.3804
ZNF721	1.28E-07	0.00055924	1.4463

Basal and insulin stimulated (100 nM, 60 min) cells from 3 donors were harvested and analyzed for mRNA expression using Next Generation Sequencing as described in Methods. Differential genes were found with the quantification data of *kallisto* [15] by the R package *DESeq2* [16] with default parameters (p-values were calculated using a two-sided Wald test and were adjusted with the method of Benjamini-Hochberg).

Supplemental Materials and Methods

Antibodies for Western Blot analysis

Antibody	Cat.No.	Vendor
AKT	#9272	Cell Signaling (Danvers, MA, USA)
pAKT-S473	#9271	Cell Signaling (Danvers, MA, USA)
GSK3a/b	#5676	Cell Signaling (Danvers, MA, USA)
pGSK3a-S21/pGSK3b-S9	#9331	Cell Signaling (Danvers, MA, USA)
PRAS40	#2610	Cell Signaling (Danvers, MA, USA)
pPRAS40-T246	#2640	Cell Signaling (Danvers, MA, USA)
mTOR	#2972	Cell Signaling (Danvers, MA, USA)
pmTOR-S2448	#5536	Cell Signaling (Danvers, MA, USA)
S6	#2217	Cell Signaling (Danvers, MA, USA)
pS6-240/244	#2215	Cell Signaling (Danvers, MA, USA)
TSC2	#4308	Cell Signaling (Danvers, MA, USA)
pTSC2-T1462	#3611	Cell Signaling (Danvers, MA, USA)
p44/42 MAPK (Erk1/2)	#9102	Cell Signaling (Danvers, MA, USA)
p44/42 pMAPK (Erk1/2)-T202/Y204	#9101	Cell Signaling (Danvers, MA, USA)
eIF4B	#3592	Cell Signaling (Danvers, MA, USA)
peIF4B-S422	#3591	Cell Signaling (Danvers, MA, USA)
GAPDH	#2118	Cell Signaling (Danvers, MA, USA)
Tubulin	#T6199	Sigma Aldrich (Saint Louis, MO, USA)
POD Goat-anti-rabbit IgG	#111-035-003	Dianova, Hamburg, Germany
POD Rabbit-anti-mouse IgG	#315-035-008	Dianova, Hamburg, Germany

References

1. Needham, E. J. *et al.* Phosphoproteomics of Acute Cell Stressors Targeting Exercise Signaling Networks Reveal Drug Interactions Regulating Protein Secretion. *Cell Rep.* **29**, 1524–1538.e6 (2019).
2. Batista, T. M. *et al.* A Cell-Autonomous Signature of Dysregulated Protein Phosphorylation Underlies Muscle Insulin Resistance in Type 2 Diabetes. *Cell Metab.* **32**, 844–859.e5 (2020).
3. Metz, K. S. *et al.* Coral: Clear and Customizable Visualization of Human Kinome Data. *Cell Syst* **7**, 347–350.e1 (2018).
4. Lund, J. *et al.* Glucose metabolism and metabolic flexibility in cultured skeletal muscle cells is related to exercise status in young male subjects. *Arch. Physiol. Biochem.* **124**, 119–130 (2018).
5. Laiman, J. *et al.* GSK3α phosphorylates dynamin-2 to promote GLUT4 endocytosis in muscle cells. *J. Cell Biol.* **222**, (2023).
6. Sano, H., Peck, G. R., Kettenbach, A. N., Gerber, S. A. & Lienhard, G. E. Insulin-stimulated GLUT4 protein translocation in adipocytes requires the Rab10 guanine nucleotide exchange factor Dennd4C. *J. Biol. Chem.* **286**, 16541–16545 (2011).
7. Lalioti, V. *et al.* The atypical kinase Cdk5 is activated by insulin, regulates the association between GLUT4 and E-Syt1, and modulates glucose transport in 3T3-L1 adipocytes. *Proc. Natl. Acad. Sci. U. S. A.* **106**, 4249–4253 (2009).
8. Yoshizaki, T. *et al.* Myosin 5a is an insulin-stimulated Akt2 (protein kinase Bbeta) substrate modulating GLUT4 vesicle translocation. *Mol. Cell. Biol.* **27**, 5172–5183 (2007).
9. Zhou, Q. L. *et al.* A novel pleckstrin homology domain-containing protein enhances insulin-stimulated Akt phosphorylation and GLUT4 translocation in adipocytes. *J. Biol. Chem.* **285**, 27581–27589 (2010).

10. Skorobogatko, Y. *et al.* RalA controls glucose homeostasis by regulating glucose uptake in brown fat. *Proc. Natl. Acad. Sci. U. S. A.* **115**, 7819–7824 (2018).
11. Chiang, S. H. *et al.* Insulin-stimulated GLUT4 translocation requires the CAP-dependent activation of TC10. *Nature* **410**, 944–948 (2001).
12. Spurlin, B. A., Park, S.-Y., Nevins, A. K., Kim, J. K. & Thurmond, D. C. Syntaxin 4 transgenic mice exhibit enhanced insulin-mediated glucose uptake in skeletal muscle. *Diabetes* **53**, 2223–2231 (2004).
13. Proctor, K. M., Miller, S. C. M., Bryant, N. J. & Gould, G. W. Syntaxin 16 controls the intracellular sequestration of GLUT4 in 3T3-L1 adipocytes. *Biochem. Biophys. Res. Commun.* **347**, 433–438 (2006).
14. Awni, W. M. & Sawchuk, R. J. The pharmacokinetics of cyclosporine. I. Single dose and constant rate infusion studies in the rabbit. *Drug Metab. Dispos.* **13**, 127–132 (1985).
15. Bray, N. L., Pimentel, H., Melsted, P. & Pachter, L. Near-optimal probabilistic RNA-seq quantification. *Nat. Biotechnol.* **34**, 525–527 (2016).
16. Love, M. I., Huber, W. & Anders, S. Moderated estimation of fold change and dispersion for RNA-seq data with DESeq2. *Genome Biol.* **15**, 550 (2014).